Electronic Supplementary Material (ESI) for Nanoscale.
This journal is © The Royal Society of Chemistry 2023

Supporting Information for

# "Covalency-aided electrochemical mechanism for $CO_2$ reduction: synergistic effect of copper and boron dual active sites drives high-efficiency ethanol product"

Shiyan Wang,*[a] Longlu Wang,[a] Xianjun Zhu,[a] Yanling Zhuang,[a] Xianghong Niu[b] and Qiang Zhao*[a]

[a] College of Electronic and Optical Engineering & College of Flexible Electronics (Future Technology), Nanjing University of Posts and Telecommunications, Nanjing 210023, China.

[b] College of Science, Nanjing University of Posts and Telecommunications, Nanjing 210023, China.

* E-mail: shiyan.wang@njupt.edu.cn; iamqzhao@njupt.edu.cn.

## Computational details

The binding energy ($E_b$) was calculated to estimate the strength of atom/molecule-surface interaction. $E_b$ could be calculated by:

$$E_b = E_{system} - E_{surf} - E_{adsorb}$$

where $E_{system}$, $E_{surf}$, and $E_{adsorb}$ are the energy of adsorption structure, surface, and adsorbent, respectively.

The formation energy of B doping Cu(100) catalyst was calculated by following formula:

$$E_f = E_{B\text{-}Cu(100)} - E_{Cu(100)} - \mu_B + \mu_{Cu}$$

where $E_{B\text{-}Cu(100)}$ is the total energies of B doping at the defective Cu(100) catalyst. $E_{Cu(100)}$ is the energy of pure Cu(100) catalyst. $\mu_B$ and $\mu_{Cu}$ are the chemical potentials of each B and Cu atom in bulk crystal, respectively.

The Gibbs reaction free energy change (ΔG) of each elementary reaction was calculated by:

$$\Delta G = \Delta E + \Delta ZPE - T\Delta S$$

where ΔE is the reaction energy determined from DFT, and ΔZPE is the difference in zero-point energies due to the reaction between the adsorbed and the gas phase by setting $H_2O$ and $H_2$ in the gas phase as reference states. ΔS is the change in entropy, computed using DFT calculations of the vibrational frequencies and standard tables for gas phase molecules. All values of ΔG were computed at T = 298 K, and pH = 0.

The limiting potential ($U_L$) was calculated as $U_L = -\Delta G_{max}/e$, where the $\Delta G_{max}$ obtained from the maximum free energy among all elementary steps of the minimum-energy pathway.

**Zero-point energy (ZPE) and entropy corrections (TS)**

The entropies of the gaseous molecules were taken from the NIST Chemistry WebBook and the zero-point energy (ZPE) was calculated according to:

$$E_{ZPE} = \sum_{i=1}^{3N} \frac{h\nu_i}{2}$$

The entropy change for adsorbed intermediates was calculated within the harmonic approximation:

$$\Delta S_{ads}(0 \rightarrow T, P^0) = S_{vib} = \sum_{i=1}^{3N} \left[ \frac{N_A h\nu_i}{T(e^{h\nu_i/K_B T} - 1)} - R\ln(1 - e^{-h\nu_i/K_B T}) \right]$$

Where $\nu_i$ is DFT-calculated normal-mode frequency for species of *3N* degree of freedom

($N$=number of atoms) adsorbed on B-Cu(100) surface, $N_A$ is the Avogadro's constant ($6.022 \times 10^{23}$ mol$^{-1}$), $h$ is the Planck's constant ($6.626 \times 10^{-34}$J s), and $k_B$ is the Boltzmann constant ($1.38 \times 10^{-23}$ JK$^{-1}$), $R$ is the ideal gas constant (8.314 J K$^{-1}$ mol$^{-1}$), and $T$ is the system temperature, and $T$=298K in this work.

The activation energy barrier ($E_{barrier}$) for the C−C coupling was calculated according to the following formula

$$E_{barrier} = E_{TS} - E_{IS}$$

where $E_{IS}$ and $E_{TS}$ are the free energy and the energy of the initial state and the transition state, respectively.

**Table S1.** Free energy corrections for gas-phase species.

| Molecule | ZPE (eV) | TΔS (eV) |
|---|---|---|
| **$CO_2$** | 0.31 | 0.66 |
| **CO** | 0.13 | 0.61 |
| **$H_2$** | 0.28 | 0.40 |
| **$H_2O$** | 0.57 | 0.67 |
| **$C_2H_4$** | 1.36 | 0.71 |
| **$C_2H_5OH$** | 2.11 | 0.83 |

**Table S2.** Calculated the energy of DFT ($E_{DFT}$), zero point energies (ZPE) and entropy (TS) of different adsorption species.

| Figures | Adsorption Species | $E_{DFT}$ (eV) | ZPE (eV) | TS (eV) |
|---|---|---|---|---|
| **Figure 3b** | B-Cu(100) | -247.88 | | |
| | OCO* | -271.69 | 0.33 | 0.12 |
| | OCOH* | -275.37 | 0.63 | 0.16 |
| | CO* | -264.49 | 0.21 | 0.13 |
| | CHO* | -267.91 | 0.48 | 0.14 |
| | HCOH* | -271.29 | 0.79 | 0.11 |
| | CH* | -260.68 | 0.35 | 0.05 |
| | $CH_2$* | -264.47 | 0.63 | 0.08 |
| | $CH_3$* | -268.43 | 0.93 | 0.13 |
| | $CH_4$ | -272.13 | 1.21 | 0.31 |
| **Figure 4c** | COCO* | -279.60 | 0.43 | 0.20 |
| | CHOCO* | -283.45 | 0.71 | 0.21 |
| | CHOCOH* | -287.40 | 1.03 | 0.22 |
| | $CH_2OHCO$* | -291.31 | 1.34 | 0.25 |
| | $CH_2CO$* | -280.72 | 0.91 | 0.15 |
| | $CH_3CO$* | -284.86 | 1.22 | 0.20 |
| | $CH_3COH$* | -288.07 | 1.51 | 0.24 |
| | $CH_3CHOH$* | -291.97 | 1.82 | 0.22 |
| | $CH_3CH_2OH$* | -295.62 | 2.16 | 0.31 |
| | CHOCO* | -282.94 | 0.69 | 0.20 |
| | CHOCHO* | -287.04 | 1.01 | 0.22 |
| | $CH_2OCHO$* | -291.07 | 1.35 | 0.17 |
| | $CH_2OHCHO$* | -294.90 | 1.67 | 0.20 |
| | $CH_2CHO$* | -284.18 | 1.18 | 0.20 |
| | $CH_2CH_2O$* | -288.28 | 1.52 | 0.14 |

| | | | | |
|---|---|---|---|---|
| **Figure 4d** | $CH_3CH_2O$* | -291.99 | 1.83 | 0.26 |
| | $CH_2CH_2OH$* | -291.93 | 1.84 | 0.21 |
| | $CH_2CH_2$* | -280.24 | 1.39 | 0.24 |
| | $CH_3CH_2OH$* | -295.62 | 2.16 | 0.31 |
| **Figure 5a** | 2B-Cu(100) | -249.02 | | |
| | 2OCO* | -297.09 | 0.65 | 0.29 |
| | 2COOH* | -304.57 | 1.28 | 0.30 |
| | 2CO* | -282.51 | 0.44 | 0.22 |
| | TS | -282.10 | 0.44 | 0.20 |
| | COCO* | -282.45 | 0.45 | 0.18 |
| | 3B-Cu(100) | -249.96 | | |
| | 3OCO* | -322.31 | 0.98 | 0.41 |
| | 3COOH* | -333.54 | 1.91 | 0.51 |
| | 3CO* | -300.41 | 0.65 | 0.38 |
| | TS | -300.24 | 0.71 | 0.21 |
| | CO*+COCO* | -300.37 | 0.65 | 0.30 |
| **Figure 5b** | 2CO* | -282.51 | 0.44 | 0.22 |
| | CO*+CHO* | -286.08 | 0.72 | 0.20 |
| | TS | -285.61 | 0.65 | 0.29 |
| | CHOCO* | -286.43 | 0.77 | 0.14 |
| | 3CO* | -300.41 | 0.65 | 0.38 |
| | 2CO*+CHO* | -304.02 | 0.93 | 0.35 |
| | TS | -303.85 | 0.94 | 0.28 |
| | CO*+CHOCO* | -304.50 | 0.99 | 0.23 |

**Table S3.** The Bader charge of the B, and the average Bader charge of nearby Cu atoms.

| | **B-Cu(100)** | **2B-Cu(100)** | **3B-Cu(100)** |
|---|---|---|---|
| **Cu** | −0.13 | −0.11 | −0.10 |
| **B** | 0.36 | 0.30 | 0.32 |

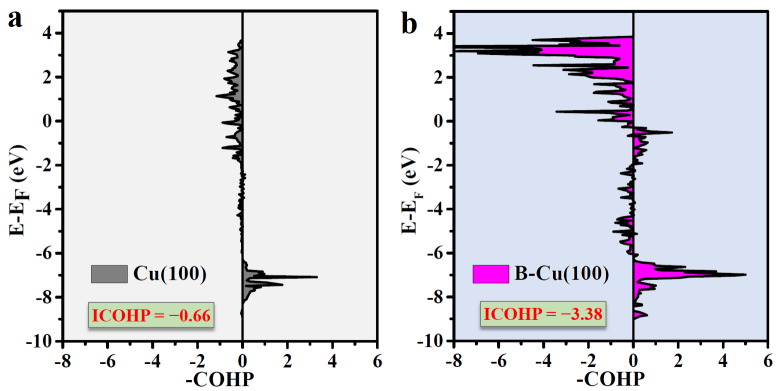


**Figure S1**. Projected crystal orbital Hamilton population (−COHP) bonding analysis of CO adsorbed on **(a)** pristine Cu(100) and **(b)** B-Cu(100), and the corresponding integrated COHP (ICOHP) value.

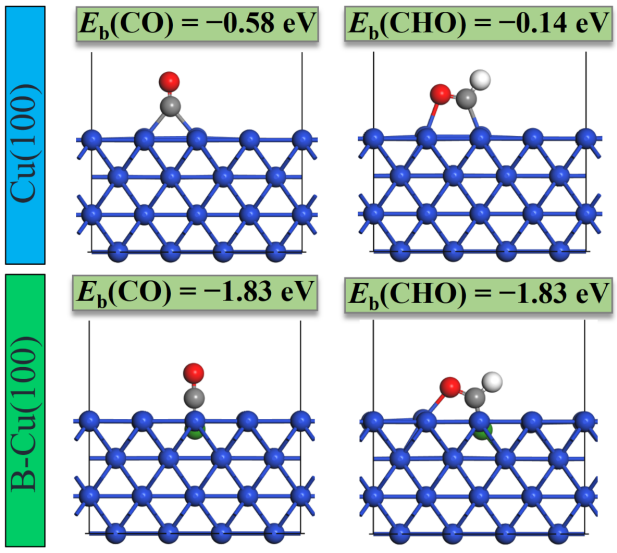


**Figure S2.** Adsorption geometries and energies of CO* and CHO* on pristine Cu(100) and B-Cu(100).

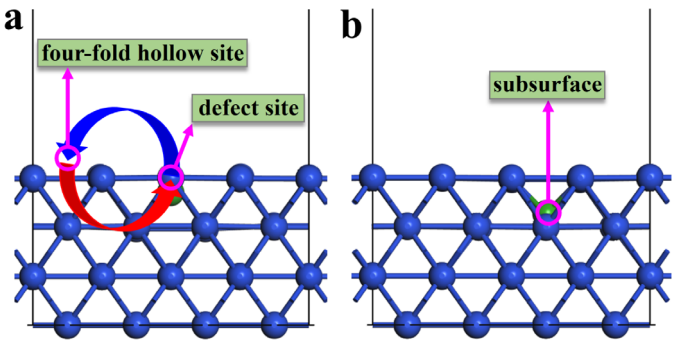


**Figure S3.** Optimized geometry structures of the B atom dopants at the defect Cu(100) **(a)** surface and **(b)** subsurface. Blue arrow: diffusion of the B atom from the defect sites to the four-fold hollow site of Cu. Red arrow: B atom from the four-fold hollow site of Cu to the defect site.

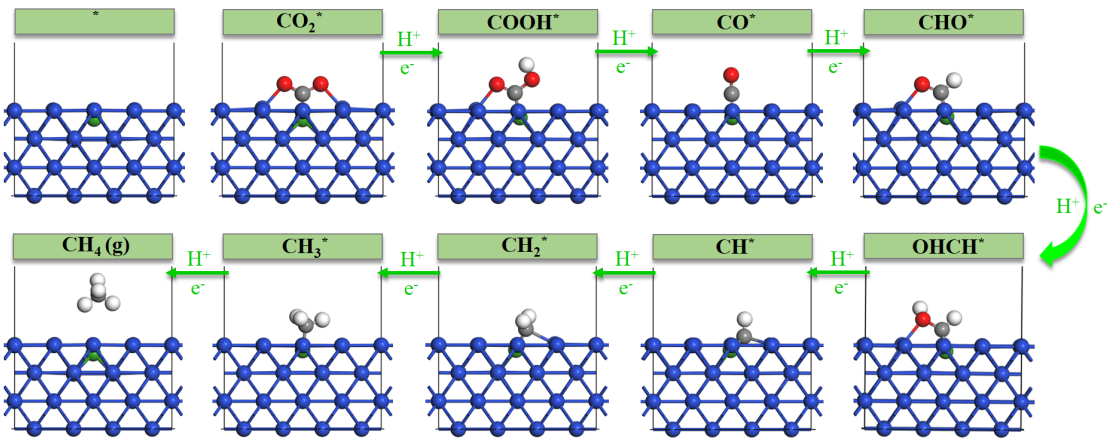


**Figure S4**. Optimized geometric of various intermediates for $CO_2$ reduction to $CH_4$ on B-Cu(100).

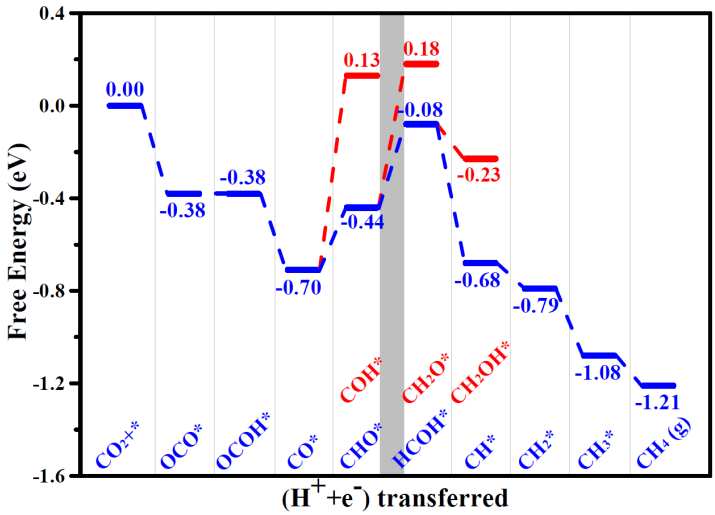


**Figure S5.** Free energy diagram of $CO_2$ reduction into $CH_4$ on B-Cu(100) catalyst. Red lines represent a competitive reaction and product selectivity.

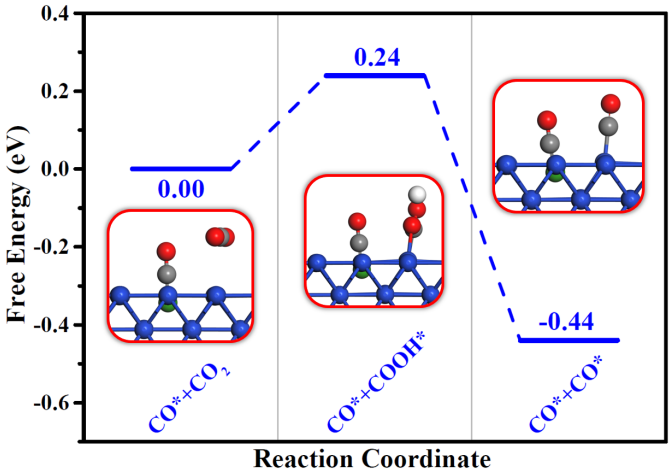


**Figure S6**. Adsorption structure and free energy diagrams for CO*+$CO_2$ conversion to CO*+CO* on B-Cu(100).

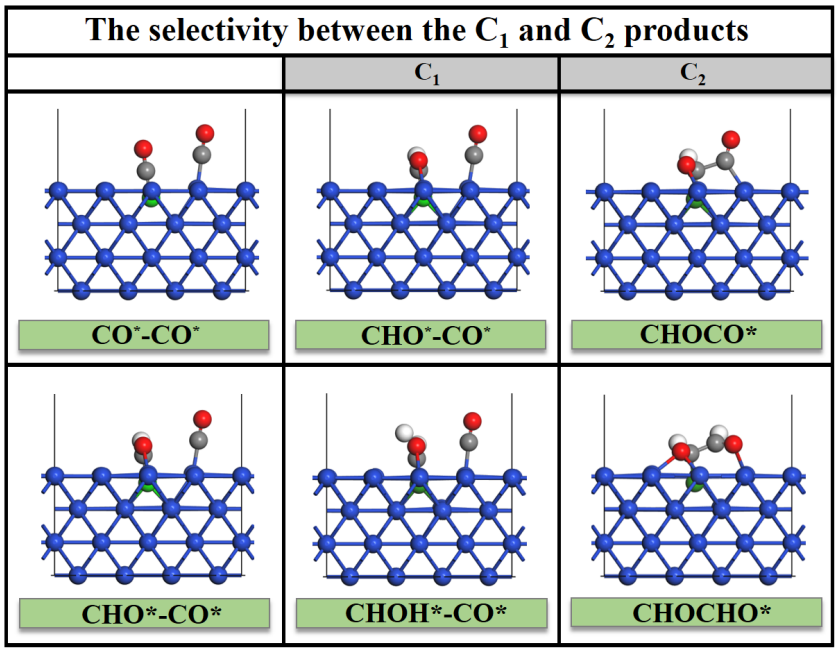


**Figure S7**. Optimized structure of the selectivity between the $C_1$ and $C_2$ products on B-Cu(100).

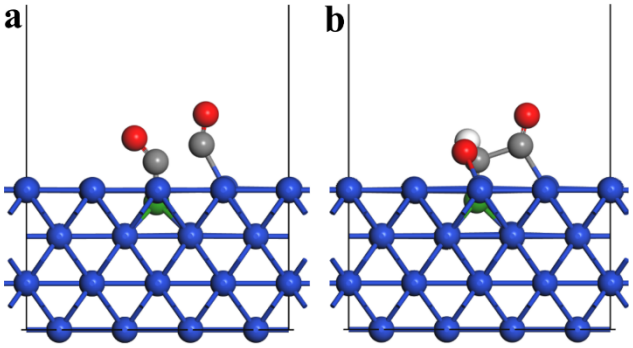


**Figure S8.** The atomic configurations of the transition state for **(a)** CO–CO and **(b)** CHO–CO coupling processes on B-Cu(100).

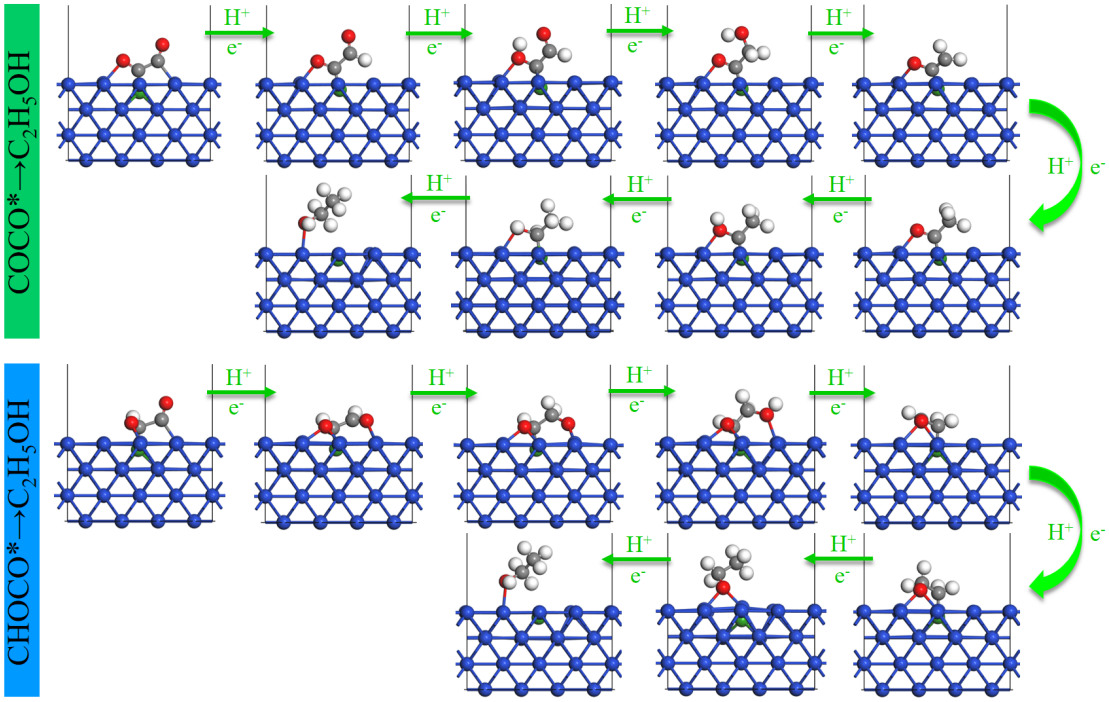


**Figure S9**. Optimized geometric of various intermediates for the hydrogenation COCO* into $C_2H_5OH$ and CHOCO* into $C_2H_5OH$.

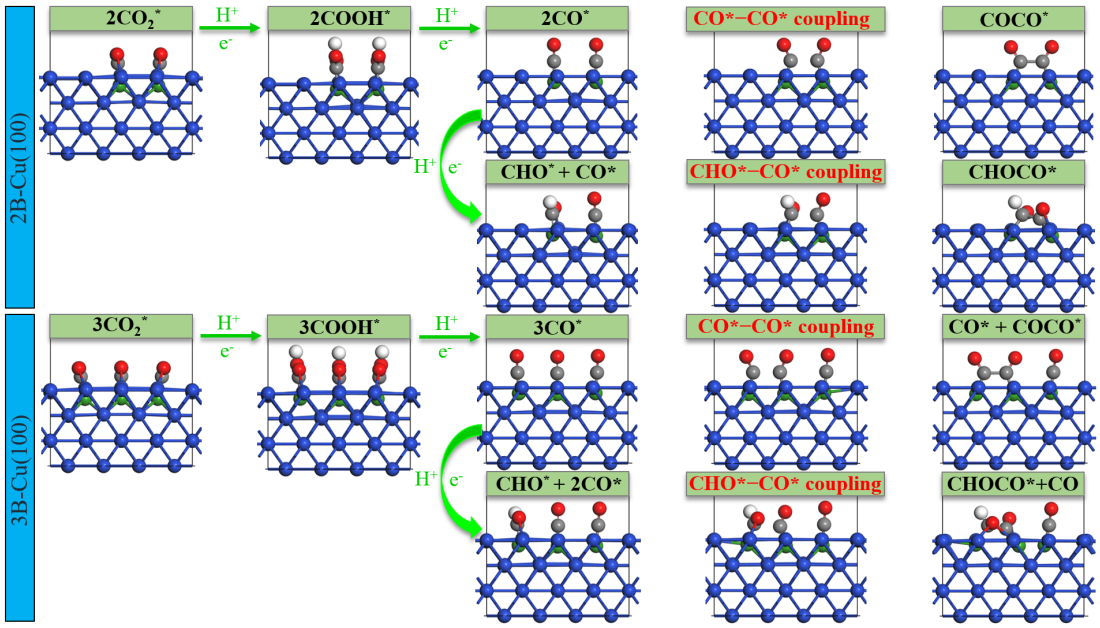


**Figure S10**. Optimized geometric of various intermediates for $CO_2$* reduction to CO* and two separated CO* dimerization to COCO* (CO*−CO* coupling), CO* hydrogenation to CHO* and CO* with CHO* dimerization to CHOCO* (CHO*−CO* coupling) on 2B-Cu(100) and 3B-Cu(100).

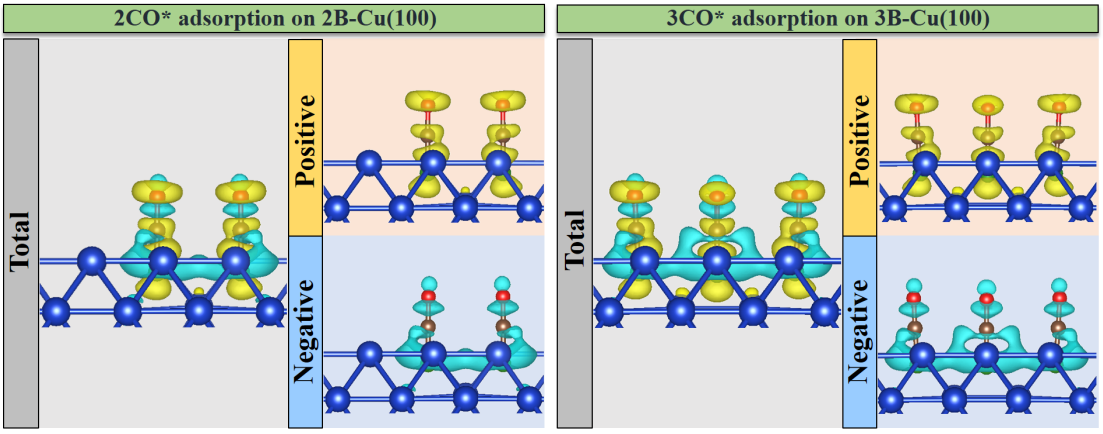


**Figure S11**. Charge density difference of CO* adsorbed on 2B-Cu(100) and 3B-Cu(100). The isosurface value is set to be 0.002 eÅ$^{-3}$. Yellow denotes electron accumulation and cyan denotes electron depletion.